Magnetism and giant magnetocaloric effect in rare-earth-based compounds R_3BWO_9 (R = Gd, Dy, Ho)

Lu-Ling Li(李炉领), Xiao-Yu Yue(岳小宇), Wen-Jing Zhang(张文静), Hu Bao(鲍虎), Dan-Dan Wu(吴丹丹), Hui Liang(梁慧), Yi-Yan Wang(王义炎), Yan Sun(孙燕), Qiu-Ju Li(李秋菊), and Xue-Feng Sun(孙学峰)

Citation: Chin. Phys. B, 2021, 30 (**7**): 077501. DOI: 10.1088/1674-1056/abf916
Journal homepage: http://cpb.iphy.ac.cn; http://iopscience.iop.org/cpb

What follows is a list of articles you may be interested in

Improvement of the low-field-induced magnetocaloric effect in $EuTiO_3$ compounds

Shuang Zeng(曾爽), Wen-Hao Jiang(姜文昊), Hui Yang(杨慧), Zhao-Jun Mo(莫兆军) Jun Shen(沈俊), and Lan Li(李岚)

Chin. Phys. B, 2020, 29 (**12**): 127501. DOI: 10.1088/1674-1056/abb230

Metamagnetic transition and reversible magnetocaloric effect in antiferromagnetic DyNiGa compound

Yan-Hong Ding(丁燕红), Fan-Zhen Meng(孟凡振), Li-Chen Wang(王利晨), Ruo-Shui Liu(刘若水), Jun Shen(沈俊)

Chin. Phys. B, 2020, 29 (**7**): 077501. DOI: 10.1088/1674-1056/ab90f3

Multicaloric and coupled-caloric effects

Jia-Zheng Hao(郝嘉政), Feng-Xia Hu(胡凤霞), Zi-Bing Yu(尉紫冰), Fei-Ran Shen(沈斐然), Hou-Bo Zhou(周厚博), Yi-Hong Gao(高怡红), Kai-Ming Qiao(乔凯明), Jia Li(李佳), Cheng Zhang(张丞), Wen-Hui Liang(梁文会), Jing Wang(王晶), Jun He(何峻), Ji-Rong Sun(孙继荣), Bao-Gen Shen(沈保根)

Chin. Phys. B, 2020, 29 (**4**): 047504. DOI: 10.1088/1674-1056/ab7da7

Magnetocaloric effect and critical behavior of the Mn-rich itinerant material Mn_3GaC with enhanced ferromagnetic interaction

Pengfei Liu(刘鹏飞), Jie Peng(彭杰), Mianqi Xue(薛面起), Bosen Wang(王铂森)

Chin. Phys. B, 2020, 29 (**4**): 047503. DOI: 10.1088/1674-1056/ab7da1

Giant low-field magnetocaloric effect in $EuTi_{1-x}Nb_xO_3$ (x=0.05, 0.1, 0.15, and 0.2) compounds

Wen-Hao Jiang(姜文昊), Zhao-Jun Mo(莫兆军), Jia-Wei Luo(罗佳薇), Zhe-Xuan Zheng(郑哲轩), Qiu-Jie Lu(卢秋杰), Guo-Dong Liu(刘国栋), Jun Shen(沈俊), Lan Li(李岚)

Chin. Phys. B, 2020, 29 (**3**): 037502. DOI: 10.1088/1674-1056/ab69e7

Magnetism and giant magnetocaloric effect in rare-earth-based compounds R_3BWO_9 (R = Gd, Dy, Ho)*

Lu-Ling Li(李炉领)[1], Xiao-Yu Yue(岳小宇)[1,†], Wen-Jing Zhang(张文静)[1], Hu Bao(鲍虎)[3], Dan-Dan Wu(吴丹丹)[1], Hui Liang(梁慧)[1], Yi-Yan Wang(王义炎)[1], Yan Sun(孙燕)[1], Qiu-Ju Li(李秋菊)[3], and Xue-Feng Sun(孙学峰)[2,1,‡]

[1] *Institute of Physical Science and Information Technology, Anhui University, Hefei* 230601, *China*
[2] *Hefei National Laboratory for Physical Sciences at Microscale, Department of Physics, and Key Laboratory of Strongly-Coupled Quantum Matter Physics (CAS), University of Science and Technology of China, Hefei* 230026, *China*
[3] *School of Physics & Material Science, Anhui University, Hefei* 230039, *China*

(Received 25 March 2021; revised manuscript received 13 April 2021; accepted manuscript online 19 April 2021)

The magnetism and magnetocaloric effect (MCE) of rare-earth-based tungstate compounds R_3BWO_9 (R = Gd, Dy, Ho) have been studied by magnetic susceptibility, isothermal magnetization, and specific heat measurements. No obvious long-range magnetic ordering can be found down to 2 K. The Curie–Weiss fitting and magnetic susceptibilities under different applied fields reveal the existence of weak short-range antiferromagnetic couplings at low temperature in these systems. The calculations of isothermal magnetization exhibit a giant MCE with the maximum changes of magnetic entropy being 54.80 J/kg·K at 2 K for Gd_3BWO_9, 28.5 J/kg·K at 6 K for Dy_3BWO_9, and 29.76 J/kg·K at 4 K for Ho_3BWO_9, respectively, under a field change of 0–7 T. Especially for Gd_3BWO_9, the maximum value of magnetic entropy change ($-\Delta S_M^{\max}$) and adiabatic temperature change ($-\Delta T_{ad}^{\max}$) are 36.75 J/kg·K and 5.56 K for a low field change of 0–3 T, indicating a promising application for low temperature magnetic refrigeration.

Keywords: magnetocaloric effect, short-range spin correlation

PACS: 75.30.Sg, 75.40.–s **DOI:** 10.1088/1674-1056/abf916

1. Introduction

Over the past few decades, materials with giant magnetocaloric effect (MCE) have received considerable attention due to their potential applications in magnetic refrigeration technology with higher energy efficiency and environment friendly.[1–4] A large MCE near room temperature can be used in the field of industrial refrigerant.[5,6] In cryogenic temperature region, a large MCE can be used for space science, medical instrumentation, and liquefaction of hydrogen and helium[7] The isothermal magnetic entropy change (ΔS_M) and adiabatic temperature change (ΔT_{ad}) under a varying external magnetic field are two main parameters to characterize the MCE. For a certain system, most of entropy change is released near the magnetic transition temperature. Thus, to achieve a large MCE at low temperature, especially for liquid-helium temperature or sub-kelvin temperature, it is necessary to search new materials with low magnetic transition temperature. In addition, a large spin quantum number, negligible magnetic anisotropy, and no thermal and field hysteresis are three key factors for giant MCE materials. Based on these considerations, the researches of MCE materials mainly focus on the rare-earth-based compounds.[8–13] Among them, Gd-based compounds exhibit remarkable performance in giant MCE at low temperature due to the large spin quantum number ($S = 7$) and no orbital angular momentum of Gd^{3+} ions. The typical examples include intermetallics Gd_3Ru,[14] perovskite oxide $GdFe_{0.5}Cr_{0.5}O_3$,[15] molecular-based complex $[Mn_4^{III}Gd_4^{III}]$Calix[4]arene,[16] frustrated antiferromagnet $SrGd_2O_4$,[17] 4f–3d spin system $GdCrTeO_6$,[18] amorphous alloy $Gd_{60}Ni_{37}Co_3$ and $Gd_{50}Co_{50}$,[19,20] etc.[21–26]

Recently, the rare-earth-based systems R_3BWO_9 (R = Gd, Dy, Ho) have attracted attention as searching for quantum spin liquid candidates.[27] These compounds crystallize in hexagonal structure with the space group $P6_3$, where the magnetic ions are connected by oxygen ions and form a distorted Kagome lattice in the *ab* plane. Along the *c* axis, the nearest neighboring rare-earth ions form a frustrated zigzag chain structure. The distance of interlayer rare-earth ions is comparable with the intralayer distance, constituting a three-dimensional framework. The magnetic property studies showed paramagnetic ground states without thermal or magnetic hysteresis in these systems.[27] Under a small applied magnetic field, the weakly coupled spins can easily rotate towards the direction of the magnetic field, accompanying a large magnetic entropy change in the magnetization process. Thus, a considerable MCE is expected in the series com-

*Project supported by the National Natural Science Foundation of China (Grant Nos. U1832209, 11874336, and 11904003), the National Basic Research Program of China (Grant No. 2016YFA0300103), the Innovative Program of Hefei Science Center CAS (Grant No. 2019HSC-CIP001), and the Natural Science Foundation of Anhui Province, China (Grant No. 1908085MA09).

†Corresponding author. E-mail: xyyue@ahu.edu.cn
‡Corresponding author. E-mail: xfsun@ustc.edu.cn

pounds.

In this paper, we studied the magnetism and MCE of R_3BWO_9 (R = Gd, Dy, Ho) compounds by using magnetic susceptibility, isothermal magnetization, and specific heat measurements. The isothermal magnetic entropy changes have been calculated according to the Maxwell thermodynamic relations. Due to the absence of long-range magnetic ordering at low temperature, a large MCE was observed in these compounds.

2. Experimental details

The polycrystalline R_3BWO_9 (R = Gd, Dy, Ho) were synthesized using standard solid-state reaction method by mixing stoichiometric amounts of high purity rare-earth oxides, H_3BO_3, WO_3, and MoO_3. In order to remove hydroxide impurity, the rare-earth oxides were dried at 900 °C for 12 hours before mixing. Then, the powders were ground together and sintered in air at 1200 °C for 72 hours with several intermediate regrindings. The purity and morphology of samples were examined by powder x-ray diffraction (XRD) at room temperature. The relative Rietveld powder diffraction profile fitting software FullProf was used to refine the crystal structure.[28] Magnetic susceptibility and isothermal magnetization were measured by using a SQUID-VSM (Quantum Design). The temperature dependence of the specific heat was measured by using a physical property measurement system (PPMS, Quantum Design) from 50 K to 2 K.

3. Results and discussion

Figure 1 shows the Rietveld refinements of powder XRD patterns for R_3BWO_9 (R = Gd, Dy, Ho) at room temperature. All samples are single phase without any detectable impurities. Table 1 lists the unit-cell parameters obtained by Rietveld refinements, which are in good agreement with the results of previous report.[27] Due to the lanthanide shrinkage, the lattice parameters decrease gradually with the decrease of the rare-earth ionic radius.

The temperature dependence of magnetic susceptibility $\chi(T)$ curves measured at different applied fields are shown in Fig. 2. At 0.1 T, no obvious magnetic transition can be observed down to 2 K for the three compounds. The corresponding inverse susceptibility $\chi^{-1}(T)$ exhibits a typical linear behavior above 50 K. Compared with Gd_3BWO_9, the relatively obvious slope changes of $\chi^{-1}(T)$ can be found around 50 K in Dy_3BWO_9 and Ho_3BWO_9, indicating the possible existence of short-range spin correlations at low temperature. Table 1 exhibits the Weiss temperatures θ_{CW} fitted by Curie–Weiss law $\chi(T) = C/(T - \theta_{CW})$ and the calculated effective magnetic moments μ_{eff} at two different temperature regimes of 100–300 K and 2–25 K. For all temperature regions, these compounds exhibit negative Weiss temperatures, revealing the dominant antiferromagnetic (AFM) exchanges between the rare-earth ions. The calculated effective magnetic moment of Gd_3BWO_9 is 7.97 μ_B at low temperature, which is close to the theoretical value 7.93 μ_B of free Gd^{3+} ions ($S = 7/2$, $g = 2.0$). For Dy_3BWO_9 and Ho_3BWO_9, the calculated effective magnetic moments are 10.44 μ_B and 10.23 μ_B, respectively, which are slightly larger than the theoretical values of free Dy^{3+} and Ho^{3+} ions.

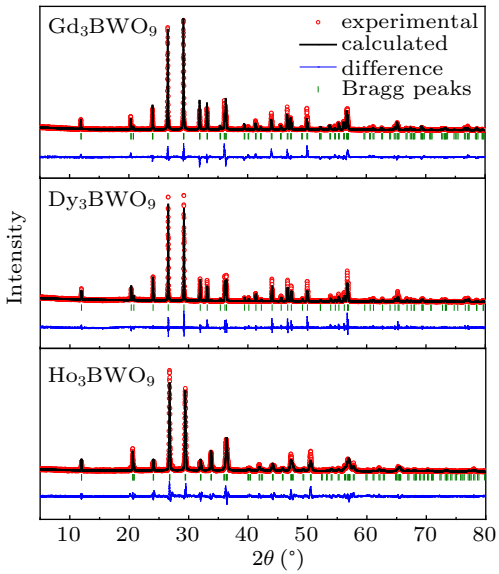

Fig. 1. The Rietveld refinements of XRD data for R_3BWO_9 (R = Gd, Dy, Ho) with experimental and calculated XRD patterns and difference between them. The vertical bars represent the expected Bragg reflection positions.

The derivative $d\chi/dT$ curves under different applied fields have been provided to further analyze the spin correlations below 20 K. As shown in the insets of Figs. 2(b), 2(d), and 2(f), a common feature is the sharp decrease of $d\chi/dT$ with decreasing temperature when $H \leq 1$ T for the three compounds. The minimum value of $d\chi/dT$ occurred at 2 K for Gd_3BWO_9 and 4 K for Dy_3BWO_9 and Ho_3BWO_9, confirming the existence of short-range spin couplings at low temperature. Beyond that, with the increase of the applied magnetic fields, the decrease of $d\chi/dT$ has been suppressed gradually, supporting a field-induced ferromagnetic (FM) transition in these systems at low temperature.

Table 1. The lattice parameters and magnetic parameters fitted by Curie–Weiss law of R_3BWO_9 (R = Gd, Dy, Ho).

Materials	a (Å)	c (Å)	High T (100–300K)		Low T (2–25 K)	
			θ_{CW} (K)	μ_{eff} (μ_B)	θ_{CW} (K)	μ_{eff} (μ_B)
Gd_3BWO_9	8.5574(3)	5.3958(4)	3.33	8.15	0.87	7.97
Dy_3BWO_9	8.5015(7)	5.3352(3)	10.99	11.27	0.73	10.44
Ho_3BWO_9	8.4714(2)	5.3078(3)	14.49	11.14	0.77	10.23

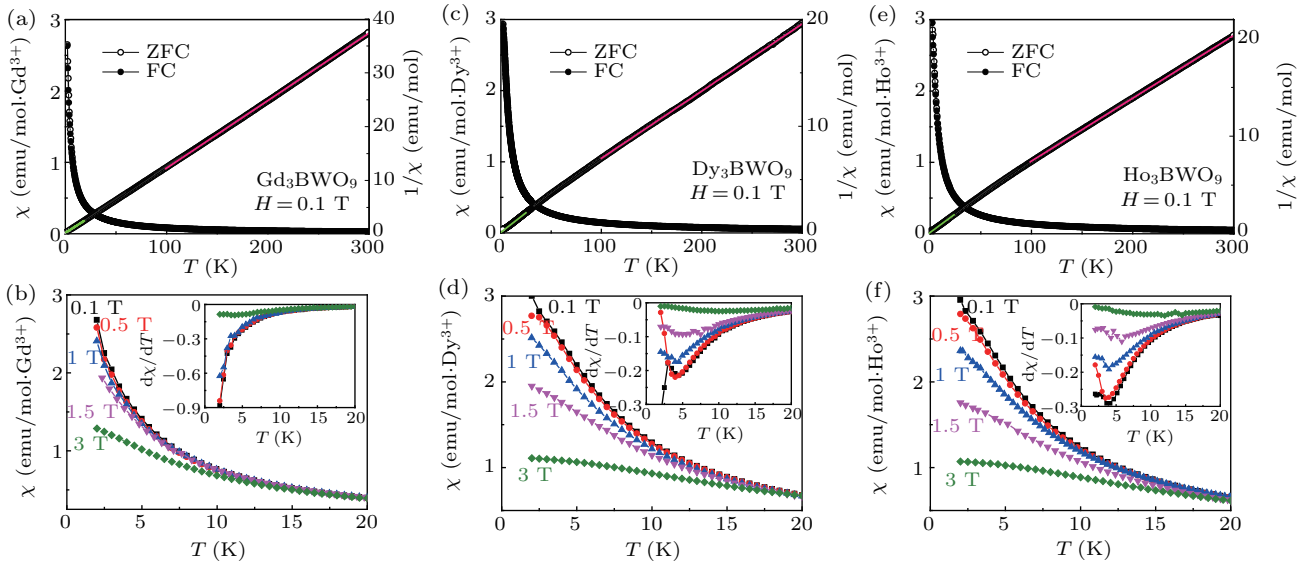

Fig. 2. Temperature dependence of susceptibility $\chi(T)$ curves under different applied magnetic fields and inverse susceptibility $\chi^{-1}(T)$ curves at 0.1 T of R_3BWO_9 (R = Gd, Dy, Ho). The pink and green solid lines indicate the Curie–Weiss fitting at different temperature regions. The insets of (a), (d), and (f) exhibit the first-order derivative $d\chi/dT$ curves under different applied magnetic fields below 20 K.

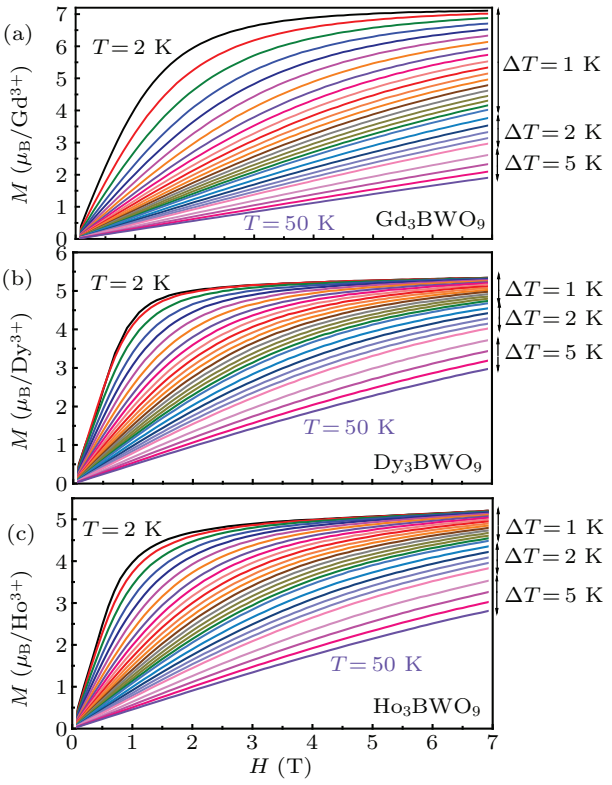

Fig. 3. The isothermal magnetization curves of R_3BWO_9 (R = Gd, Dy, Ho) measured at different temperatures.

Figure 3 shows the isothermal magnetization curves of R_3BWO_9 (R = Gd, Dy, Ho) measured from 2 K to 50 K with different temperature steps. The magnetization increases smoothly with increasing magnetic field and no field hysteresis was observed for the whole temperature range. Here, only the H-increasing curves are presented in Fig. 3. With increasing temperature, the magnitude and curvature of the magnetization curve decrease, suggesting a strong effect of thermal perturbation on spin alignment. For Gd_3BWO_9, the magnetic moment at 2 K and 7 T is derived to be 7.11 μ_B, which is close to the saturated magnetic moment of free Gd^{3+} ions. For Dy_3BWO_9 and Ho_3BWO_9, the maximum magnetic moments at 2 K are 5.50 μ_B and 5.37 μ_B, respectively.

According to the isothermal magnetization curves, the magnetic entropy change ΔS_M can be calculated by integrating the Maxwell's equation $\Delta S_M = \int_0^H (\partial M/\partial T)dH$. The temperature dependence of $-\Delta S_M$ for different applied fields is shown in Fig. 4. For Gd_3BWO_9, the value of $-\Delta S_M$ increases monotonously with decreasing temperature and reaches 36.75 J/kg·K and 54.80 J/kg·K at 2 K for field ranges of 0–3 T and 0–7 T, respectively (see Fig. 4(a)). Especially for a relatively small field change of 0–2 T, the value of $-\Delta S_M^{max}$ is 25.13 J/kg·K, which is highly desired for practical applications of MCE materials. For Dy_3BWO_9 and Ho_3BWO_9, the temperature dependence of $-\Delta S_M$ under different field changes exhibits similar behavior, as shown in Figs. 4(b) and 4(c). The values of $-\Delta S_M$ increase monotonously with decreasing temperature and reach 28.50 J/kg·K at 6 K for Dy_3BWO_9 and 29.76 J/kg·K at 4 K for Ho_3BWO_9, under a field change of 0–7 T. Compared with Gd_3BWO_9, Dy_3BWO_9 and Ho_3BWO_9 exhibit relatively smaller magnetic entropy changes and higher characteristic temperatures of $-\Delta S_M^{max}$ under the same field change. It should be noted the crystalline electric field (CEF) effect of Dy^{3+} and Ho^{3+} ions can also have significant influence on the anisotropy magnetic interaction and magnetic ground state at low temperature. However, since the effective magnetic moments are very close to those of the free rare-earth ions, as shown in Table 1, the CEF may have negligibly small effect on the magnetic properties of the present materials. The relatively higher characteristic temperatures of $-\Delta S_M^{max}$ in Dy_3BWO_9 and Ho_3BWO_9 may originate from the

spin correlations below 50 K, in accordance with the analysis of magnetic susceptibility (see Fig. 2). In addition, the characteristic temperature of $-\Delta S_{\rm M}^{\rm max}$ for Dy_3BWO_9 shifts to high temperature with the increase of field change. The insets of Figs. 4(b) and 4(c) provide the corresponding magnetic dependence of refrigerant capacity (RCP) for Dy_3BWO_9 and Ho_3BWO_9. The RCP defined as $\Delta S_{\rm M}^{\rm max}\delta_{\rm FMHM}$, is an important quality factor to measure the amount of heat transfer in an ideal refrigeration cycle, where $\delta_{\rm FMHM}$ is the full width at half of $-\Delta S_{\rm M}$ curves The obtained RCP is 358 J/kg for Dy_3BWO_9 and 384 J/kg for Ho_3BWO_9 with a field change of 0–7 T, respectively.

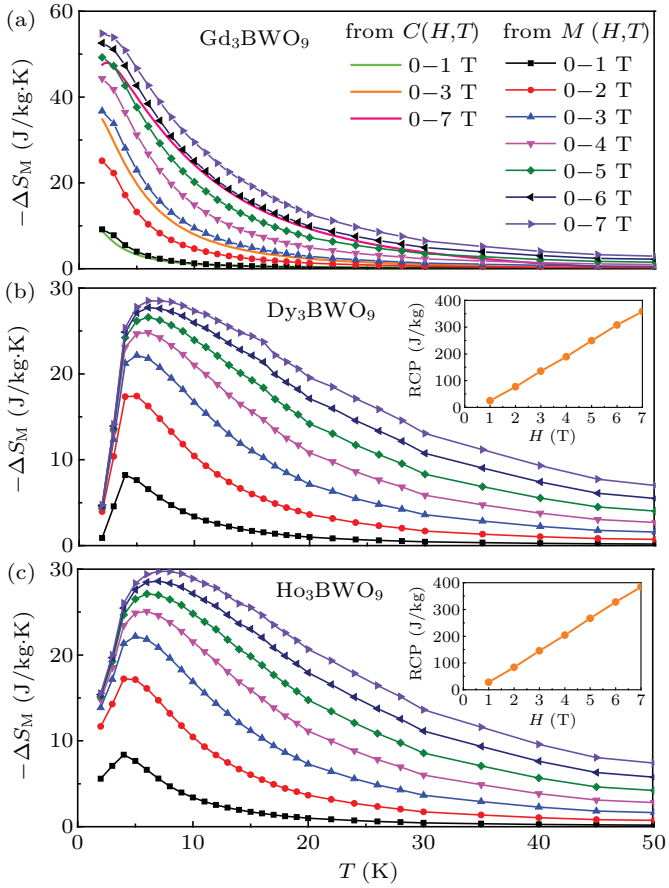

Fig. 4. Temperature dependence of magnetic entropy change $-\Delta S_{\rm M}$ for R_3BWO_9 (R = Gd, Dy, Ho), respectively. The insets of (b) and (c) give the RCP as a function of magnetic field.

In order to further investigate the MCE of Gd_3BWO_9, the specific heat has been measured from 50 K to 2 K. The temperature dependence of the specific heat under different applied magnetic fields is shown in Fig. 5(a). The zero-field specific heat data indicates the absence of long-range magnetic order down to 2 K, in agreement with the results of magnetic susceptibility, but exhibits an upturn at $T < 8$ K. With increasing fields, a broad peak appears around 5 K for $H = 3$ T and shifts to higher temperatures gradually. Similar with $GdCrTiO_5$ and $BiGdO_3$, such behaviors indicate the existence of short-range spin correlations at low temperature in this system.[25,29] The background specific heat of phonon contribution can be described by $C_{\rm ph} = \beta T^3 + \beta_5 T^5 + \beta_7 T^7$ with $\beta = 112 \times 10^{-3}$ J/mol·K^4, $\beta_5 = -4.66 \times 10^{-7}$ J/mol·K^6, $\beta_7 = 7.40 \times 10^{-11}$ J/mol·K^8. By integrating $(C_{\rm p} - C_{\rm ph})/T$ from 50 K to 2 K, the temperature dependence of the magnetic entropy is obtained and shown in Fig. 5(b). The obtained values of magnetic entropy are 6.4 J/mol·K for $H = 0$ and 38.5 J/mol·K for $H = 7$ T, which are 12% and 74% of the theoretically maximum magnetic entropy $3R\ln 8$ for fully polarized Gd^{3+} ions, respectively. The small change of entropy at zero field confirms the existence of spin correlations below 2 K.

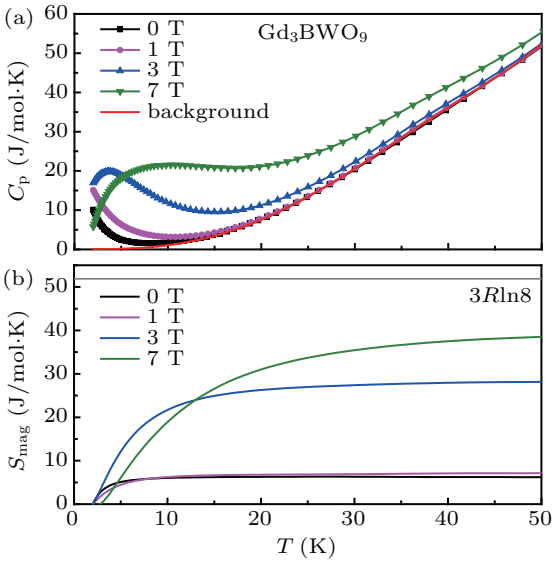

Fig. 5. (a) Temperature dependence of the specific heat measured at different magnetic fields for Gd_3BWO_9. The red line represents the phonon contribution. (b) The temperature dependence of magnetic entropy $S_{\rm mag}$.

Based on the temperature dependence of the specific heat curves under different applied magnetic fields, the magnetic entropy change of Gd_3BWO_9 can be calculated using the equation

$$\Delta S_{\rm M} = \int_0^T \frac{C(T,H_1) - C(T,H_0)}{T}\,{\rm d}T.$$

As shown in Fig. 4(a), the temperature dependences of $\Delta S_{\rm M}$ calculated from isothermal magnetization $M(T,H)$ and specific heat $C(T,H)$ exhibit same tendency. The adiabatic temperature change $\Delta T_{\rm ad}$ as another important parameter to characterize the MCE materials can be calculated by using the equation

$$\Delta T_{\rm ad} = -\int_0^H \frac{T}{C_{\rm p}(H)}\left(\frac{\partial M}{\partial T}\right){\rm d}H.$$

Figure 6 shows the temperature dependence of $-\Delta T_{\rm ad}$ for Gd_3BWO_9. Due to the existence of short-range spin correlations and field-induced FM transition, the characteristic temperature of $-\Delta T_{\rm ad}^{\rm max}$ shifts towards higher temperature with increasing field and reaches 2.86 K, 5.56 K, and 9.16 K with the field changes of 0–1 T, 0–3 T, and 0–7 T, respectively. Table 2 provides a comparison of magnetic entropy changes with some Gd-based oxides for the same magnetic field ranges of 1 T,

3 T, and 7 T. The $-\Delta S_M$ values of Gd_3BWO_9 are comparable or even larger than those of many Gd-based oxides within the same magnetic field region.

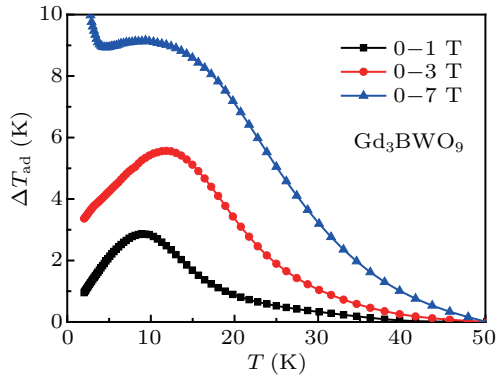

Fig. 6. Temperature dependence of adiabatic temperature change $-\Delta T_{ad}$ for Gd_3BWO_9.

Table 2. A comparison of the MCE between Gd_3BWO_9 and some other Gd-based oxides under the magnetic field changes of 1 T, 3 T, and 7 T.

Materials	ΔS_M (J/kg·K)			
	1 T	3 T	7 T	Ref.
$GdPO_4$	~ 24.00	~ 50.00	62.00	[10]
$GdCrTeO_6$	10.90	30.30	41.80	[18]
$GdMnO_3$	1.60	6.80	15.40	[21]
$GdCrO_4$	7.70	16.50	28.30	[22]
$GdFeO_3$	1.70	16.20	44.00	[23]
$BiGdO_3$	~ 1.30	~ 8.00	25.00	[25]
$GdFeTeO_6$	10.90	23.60	38.50	[26]
Gd_3BWO_9	9.22	36.75	54.80	this work

Compared with the magnetic order systems, the rare-earth ions in R_3BWO_9 (R = Gd, Dy, Ho) are located in a three-dimensional frustrated framework, which may enhance the disorder of spins at low temperature. These weakly coupled spins can easily rotate towards the direction of magnetic field and generate a large magnetic entropy change under a small applied magnetic field. Thus, rare-earth-based oxides R_3BWO_9 (R = Gd, Dy, Ho) can be considered as the potential magnetic refrigerant materials at low temperature without field and thermal hysteresis in the magnetization process.

4. Summary

In summary we have synthesized a series of rare-earth-based boron tungstate compounds R_3BWO_9 (R = Gd, Dy, Ho) by the solid-state reaction method. All three compounds exhibit no long-range magnetic order down to 2 K. Under an external magnetic field, the weakly AFM coupled spins can rotate towards the direction of the applied field and yield a large MCE. For a field range of 0–7 T, the maximum values of the magnetic entropy change reach 54.80 J/kg·K at 2 K for Gd_3BWO_9, 28.50 J/kg·K at 6 K for Dy_3BWO_9, and 29.76 J/kg·K at 4 K for Ho_3BWO_9. Especially for Gd_3BWO_9, the value of $-\Delta S_M^{max}$ is 25.13 J/kg·K at 2 K with a small field change of 0–2 T. Without the thermal and field hysteresis, R_3BWO_9 (R = Gd, Dy, Ho) can be considered as potential candidate materials for magnetic refrigeration at low temperature.

References

[1] Matsunami D, Fujita A, Takenaka K and Kano M 2015 *Nat. Mater.* **14** 73

[2] Balli M, Jandl S, Fournier P and Dimitrov D Z 2016 *Appl. Phys. Lett.* **108** 102401

[3] Balli M, Jandl S, Fournier P and Kedous-Lebouc A 2017 *Appl. Phys. Rev.* **4** 021305

[4] Franco V, Bláquez J S, lpus J J, Law J Y, Moreno-Ramíez L M and Conde A 2018 *Prog. Mater. Sci.* **93** 112

[5] Brown G V 1976 *J. Appl. Phys.* **47** 3673

[6] Gschneidner Jr K A, Pecharsky V K and Tsokol A O 2005 *Rep. Prog. Phys.* **68** 1479

[7] Numazawa T, Kamiya K, Utaki T and Matsumoto K 2014 *Cryogenics* **62** 185

[8] Pakhira S, Mazumdar C, Ranganathan R and Avdeev M 2017 *Sci. Rep.* **7** 7367

[9] Lorusso G, Sharples J W, Palacios E, Roubeau O, Brechin E K, Sessoli R, Rossin A, Tuna F, McInnes E J L, Collison D and Evangelisti M 2013 *Adv. Mater.* **25** 4653

[10] Palacios E, Rodríguez-Velamazán J A, Evangelisti M, Mclntyre G J, Lorusso G, Visser D, de Jongh L J and Boatner L A 2014 *Phys. Rev. B* **90** 214423

[11] Li L, Nishimura K, Hutchison W D, Qian Z, Huo D and NamiKi T 2012 *Appl. Phys. Lett.* **100** 152403

[12] Wang W, Li Y, Li L, Li Q, Wang D, Zhu J, Li J and Zeng M 2021 *J. Phys.: Condens. Matter* **33** 015802

[13] Balli M, Jandl S, Fournier P, Vermette J and Dimitrov D Z 2018 *Phys. Rev. B* **98** 184414

[14] Monteiro J C B, dos Reis R D and Gandra F G 2015 *Appl. Phys. Lett.* **106** 194106

[15] Yin L H, Yang J, Tong P, Luo X, Song W H, Dai J M, Zhu X B and Sun Y P 2017 *Appl. Phys. Lett.* **110** 192904

[16] Karotsis G, Kennedy S, Teat S J, Beavers C M, Fowler D A, Morales J J, Evangelisti M, Dalgarno S J and Brechin E K 2010 *J. Am. Chem. Soc.* **132** 12983

[17] Jiang X, Ouyang Z W, Wang Z X, Xia Z C and Rao G H 2018 *J. Phys. D: Appl. Phys.* **51** 045001

[18] Liu J D, Ouyang Z W, Liu X C, Cao J J, Wang Z X, Xia Z C and Rao G H 2020 *J. Appl. Phys.* **127** 173902

[19] Ma Y F, Tang B Z, Xia L and Ding D 2016 *Chin. Phys. Lett.* **33** 126101

[20] Tang B Z, Liu X P, Li D M, Yu P and Xia L 2020 *Chin. Phys. B* **29** 056401

[21] Mahana S, Manju U and Topwal D 2017 *J. Phys. D: Appl. Phys.* **50** 035002

[22] Midya A, Khan N, Bhoi D and Mandal P 2014 *J. Appl. Phys.* **115** 17E114

[23] Das M, Roy S and Mandal P 2017 *Phys. Rev. B* **96** 174405

[24] Dey K, Indra A, Majumdar S and Giri S 2017 *J. Mater. Chem. C* **5** 1646

[25] Dutta A, Jana R, Mukherjee G D and Das I 2020 *J. Alloys Compd.* **846** 156221

[26] Lei D D, Ouyang Z W, Yue X Y, Yin L, Wang Z X, Wang J F, Xia Z C and Rao G H 2018 *J. Appl. Phys.* **124** 233904

[27] Ashtar M, Guo J, Wan Z, Wang Y, Gong G Liu Y, Su Y and Tian Z 2020 *Inorg. Chem.* **59** 5368

[28] McCusker L B, Von Dreele R B, Cox D E, Louër D and Scardi P 1999 *J. Appl. Cryst.* **32** 36

[29] Basu T, Singh K, Gohil S, Ghosh S and Sampathkumaran E V 2015 *J. Appl. Phys.* **118** 234103